

Polyaniline for Improved Blue Energy Harvesting: Highly Rectifying Nanofluidic Diodes Operating in Hypersaline Conditions via One-Step Functionalization

Gregorio Laucirica, María Eugenia Toimil-Molares, Christina Trautmann, Waldemar Marmisollé,* and Omar Azzaroni*



Cite This: *ACS Appl. Mater. Interfaces* 2020, 12, 28148–28157



Read Online

ACCESS |



Metrics & More



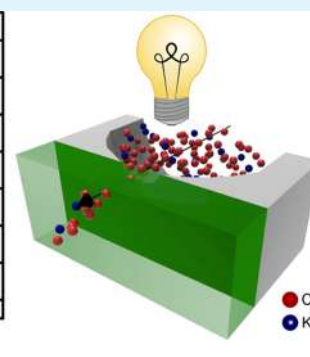
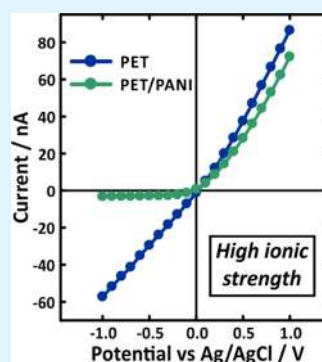
Article Recommendations



Supporting Information

ABSTRACT: Solid-state nanochannels have attracted substantial attention of the scientific community due to their remarkable control of ionic transport and the feasibility to regulate the iontronic output by different stimuli. Most of the developed nanodevices are subjected to complex modification methods or show functional responsiveness only in moderate-ionic-strength solutions. Within this project, we present a nanofluidic device with enhanced ionic current rectification properties attained by a simple one-step functionalization of single bullet-shaped polyethylene terephthalate (PET) nanochannels with polyaniline (PANI) that can work in high-ionic-strength solutions. The integration of PANI also introduces a broad pH sensitivity, which makes it possible to modulate the ionic transport behavior between anion-selective and cation-selective regimes depending on the pH range. Since PANI is an electrochemically active polymer, ionic transport also becomes dependent on the presence of redox stimuli in solution. We demonstrate that PANI-functionalized single-nanochannel membranes function as an efficient salinity gradient-based energy conversion device even in acidic concentrated salt solutions, opening the door to applications under a variety of novel operating conditions.

KEYWORDS: nanochannels, polyaniline, nanofluidic diodes, hypersaline compatibility, salinity gradient power, salinity gradient power, osmotic power generation



INTRODUCTION

Scaling down to the nanometric range reveals several phenomena that do not operate on a micrometric scale. For this reason, and exploiting technological advances in nanofluidics, the study of solid-state nanochannels (SSNs) has attracted much attention in recent years.^{1,2} The accurate control of ionic transport in confined geometries combined with fascinating size-dependent properties have promoted the design of SSN with different applications such as biosensing, energy conversion, and filtration, among many others.^{3–7} Furthermore, fully abiotic nanochannels offer some advantages over ion biological channels, such as tailored size and chemical stability, which allows, for example, the exposition of nanochannels to a wide range of experimental conditions: extreme pH electrolyte values, high ionic concentrations, high temperatures, organic solvents, etc. Among the various techniques employed to produce SSNs, ion-track technology enables the reproducible fabrication of polymer nanochannels with tailored geometries and well-adjusted size.^{8,9} Moreover, the chemical etching of the ion-tracks exposes carboxylate groups on the inner walls of the resulting nanochannels, which

facilitates subsequent chemical modifications. This, in turn, enables the intentional integration of a variety of specific chemical functionalities to the polymer nanochannels, resulting in nanofluidic platforms for which the ionic transport is modulated by several stimuli such as light, temperature, pH, and specific chemical moieties, among others, in a similar way to biological ion channels.^{10–12} In this context, the exploration of new strategies to integrate functional systems to solid-state nanochannels is a task of significant relevance.^{9,13}

In addition, the ability to easily obtain ionic current rectifying devices in fully abiotic nanochannels is a very interesting feature of the ion-track-etching method.¹⁴ The ionic current rectification (ICR) implies that the ionic flux is favored at one polarity voltage (diode-like transport). Rectifying

Received: March 18, 2020

Accepted: May 25, 2020

Published: May 25, 2020



nanochannels have I – V curves characterized by a low-conductance branch and a high-conductance branch. Devices with this asymmetric transport have been widely studied for a variety of applications such as nanofluidic diodes and chemical sensors.^{3,15} Rectification is based on the rupture of electric potential symmetry, which can be achieved using different approaches.^{10,16} Usually, this non-ohmic transport is obtained by the design of asymmetric-shaped charged nanochannels. In these cases, the narrow aperture (tip) must have a comparable dimension to the Debye length.^{17–19} This fact introduces limitations to both the fabrication and operation of the device: nanometer-sized channels and moderate salt concentrations are required. Referring to the first issue, Siwy and co-workers have recently emphasized the importance of developing rectifying devices with a high tip diameter/Debye length ratio.^{20,21} They obtained a rectifying device in moderate ionic strength using a conical microchannel with the tip region filled with high-molecular-weight poly-L-lysine. Concerning the issue related to the salt concentration in operation solutions, the nanometric-sized channels usually lose their rectifying behavior or show only low rectification efficiency in symmetric KCl concentrations greater than 1 M, i.e., where the Debye length is drastically decreased. This condition limits the application of nanofluidic diodes to high-salt-concentration solutions.^{22,23} To overcome this limitation, two main strategies have been proposed: decreasing the small tip opening of the nanochannels below 10 nm (which is a challenge for the fabrication and reproducibility of the process) or employing complex multistep modification methods.^{23–26} Another common way to design rectifier devices is the asymmetric modification of nanochannels.^{15,27,28} The synergism between asymmetric modification and asymmetric geometry has been introduced previously. Vlassiok and Siwy developed a bipolar diode based on a modified conical nanochannel by exposing only the tip side of the nanochannel to the reaction mixture.¹⁵ They obtained a nanochannel with a patterned surface, which conferred high rectification efficiency. This design approach is very versatile as the modification with appropriate functional systems allows incorporating other interesting properties, such as zwitterionic behavior, gating, and selectivity.^{29,30} However, the loss of rectification at high ionic strength was still a critical issue.

Related to the ionic current rectification behavior, an interesting application of SSNs is their use in ion-selective membranes to generate an energy of low environmental impact via reverse electrodialysis, which is an attractive approach to global problems associated with energy generation and pollution.^{23,31,32} Several works have evidenced the capability of track-etched nanochannels to achieve this goal.^{31,33–35} Nevertheless, the exploration of new modification methods that allow the development of salinity gradient power (SGP) generators is still scarce. In addition, SGP systems are effective at pH conditions that ensure an appreciable surface charge (typically $\text{pH} > 6$), and, generally, the applications are limited to solutions with moderate ionic strength.^{31,34,36} In this sense, the design of SGP systems able to operate under different conditions could allow the exploitation of diverse salinity wastes for energy generation.³⁷ To tackle these goals, the authors have proposed different approaches such as the functionalization with highly charged molecular systems and interfacial design. On one side, the rational choice of a modifying agent is crucial since its nature determines the operative conditions of the SGP generator. On the other hand,

in the past years, the interfacial design has been shown to be a key factor to achieve a successful scaling-up from single-pore to multipore systems.^{38,39}

In our project, we focus on surface modification of nanochannels with polyaniline (PANI), which is a widespread electroactive polymer obtained by either electrochemical or chemical oxidation of aniline.⁴⁰ According to the experimental conditions, PANI can exist in three redox states: *leucoemeraldine* (LE), *emeraldine* (E), and *pernigraniline*.⁴¹ The redox states are defined by different ratios of secondary amine and imine groups, with different associated acid–base equilibria. Thus, the ionic charge of PANI can be tuned by changing the pH of the solution and the concentration of redox agents. The coupling between acid–base and redox processes in PANI^{42,43} has been recently exploited for the construction of a redox-responsive iontronic device based on the electropolymerization of PANI on Au-sputtered single-pore track-etched nanochannels. In this system, variations in the PANI electrostatic charge, caused by both pH changes and applied potential, affected the iontronic behavior, as revealed by changes in the I – V iontronic response.⁴⁴ In contrast, in the present work, we developed a functionalization method that avoids both previous metallization and electropolymerization steps and allows the integration of a PANI film directly on track-etched polyethylene terephthalate (PET) foils by chemical synthesis, which greatly reduces the complexity of the whole-membrane fabrication process. We show that this simple modification method of bullet-shaped single-nanochannel membranes with PANI provides pH- and redox-responsive nanofluidic channels with significant rectification properties even when operating in high-ionic-strength solutions (up to saturated KCl solutions). This one-step chemical functionalization of track-etched PET foils allowed creating asymmetric membranes with enhanced performance as an energy conversion system based on reverse electrodialysis in high-salt-concentration media by combining the advantages of the bullet-shaped nanochannels in terms of rectification and energy-harvesting ability with the appropriate interfacial design for producing enhanced SGP generation.

Results and Discussion. *PANI Functionalization and Membrane Characterization.* PET membranes (12 μm thick) were irradiated with a single high-energy heavy ion (2.2 GeV Au ions) at the UNILAC accelerator of the GSI Helmholtz Centre for Heavy Ion Research. In polymer foils, each individual ion of such high energy produces a so-called ion track, a cylindrical damage trail, a few nanometers in diameter and several tens of micrometers in length. Under appropriate conditions, the tracks in the irradiated foils can be dissolved and converted into a bullet-shaped channel with a nanometric tip diameter (more details are described in the [Supporting Information \(SI\)](#)).⁴⁵ After etching, the membranes exhibit a cation-driven rectification due to the negative charge of surface carboxylate groups created during the etching. This response is typical of an asymmetric channel with a nanometric tip diameter ($d_{\text{tip}} \sim 70$ nm; [Figure S1](#)) and negatively charged walls ([Figure 1](#)). The low current of the nonmodified channel is explained by the low ratio of the carboxylate groups dissociated at $\text{pH} = 4$. For PANI functionalization, the tip side of the foil was exposed to a mixture of ammonium persulfate (APS) and aniline in 0.5 M H_2SO_4 for 3 h ([Figure 1A](#)). Under these conditions, a PANI film was formed on the tip side of the PET membrane.⁴⁶ Scanning electron microscopy (SEM) was applied to investigate the configuration of the PANI film modification. In contrast to the electropolymerization of PANI

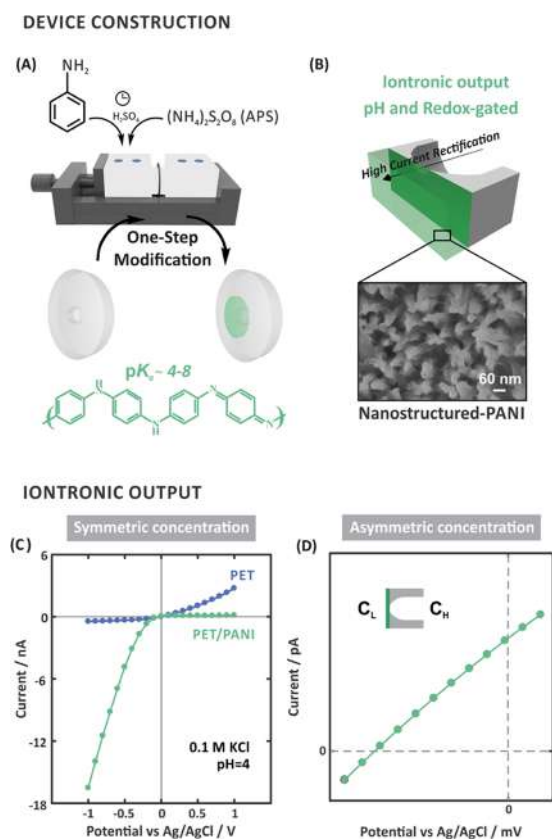


Figure 1. (A) Scheme of an etching cell, which also serves for the asymmetric modification of the single-nanochannel membrane with PANI, by adding the polymerization mixture on the tip side. (B) Scheme of the asymmetric membrane with the bullet-shaped nanochannel coated by PANI on the tip side (green) (top) and SEM image of PANI film (bottom). (C) Typical $I-V$ curves of the PET foil with a single nanochannel before (blue) and after (green) PANI modification recorded in 0.1 M KCl, pH = 4 (symmetrical). The high rectification in PET/PANI is ascribed to the charged state of the protonated PANI ($\text{pK}_a > 4$). (D) $I-V$ curve of a PANI-modified foil recorded under asymmetrical electrolyte conditions (tip side: 0.1 M KCl, low concentration C_L ; base side: 1 M KCl, high concentration C_H) at pH = 3.5.

on Au-sputtered membranes in which the generation of a polymer film from the metallized walls produces a decrease of the nanochannel diameter,⁴⁴ the present chemical synthesis leads to the formation of a dense PANI film on top of the membrane (Figures 1B and S1). Moreover, the synthetic approach developed here ensures that the nanochannels are not filled with the polymer as aniline is not transported through the track-etched PET nanochannels under acidic conditions (pH < 6).⁴⁷ Instead of depositing polymer on the walls of the nanochannel, our functionalization approach leads to the coating of the tip side of the PET foil with a PANI film.

After modification, the iontronic output recorded under symmetrical electrolyte conditions (KCl = 0.1 M) shows a high anion-driven rectification (rectification triggered by positive surface charge) at pH = 4, which is attributed to the high-positive-charge state of PANI ($\text{pK}_a > 4$) (Figure 1C). Earlier studies and PNP simulations ascribed the ionic rectification in SSN to the combination of surface charge and asymmetric geometry (e.g., bullet-shaped nanochannels), yielding accumulation or depletion of ions depending on the polarity of the transmembrane voltage. This fact explains the low- and high-

conductance branches in the $I-V$ curves. Our approach tackles both criteria, surface charge and geometry of the nanochannel, by a simple one-step chemical synthesis on the tip side, providing a system with outstanding rectification performance. On the other hand, the iontronic output recorded under asymmetrical electrolyte conditions (0.1 M KCl at the tip side; 1 M KCl at the base side) shows a shift of the curve from the origin, which is originated by the anion selectivity of the PANI film (Figure 1D). This behavior is crucial in the development of SGP generators, and, for this reason, it will be addressed in more detail in the Blue Energy Harvesting Performance section.

The etched PET foils and the PANI-modified PET (PET/PANI) foils were further characterized by UV-vis, Raman, and X-ray photoelectron spectroscopies (XPS) and contact angle measurements. The results are summarized in Figure 2. The

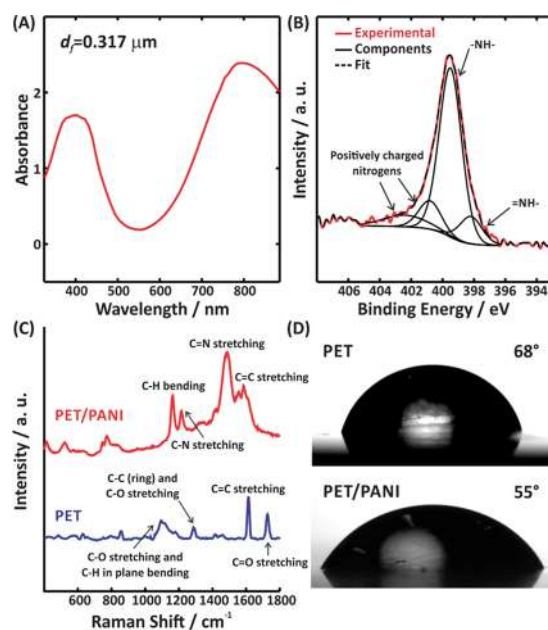


Figure 2. Characterization results of a PET membrane with and without PANI modification. (A) UV-vis spectrum of a PET/PANI membrane at pH = 3. The film thickness was determined from the absorbance value at $\lambda = 400$ nm. (B) XPS spectrum of PET/PANI in the region of the N 1s binding energy. The peak was deconvoluted into four components. (C) Raman spectra of PET (blue) and PET/PANI foils (red). (D) Contact angle images of PET and PET/PANI foils.

UV-vis spectrum of a representative PET/PANI foil in acidic KCl solution shows absorption bands at 400 and 800 nm, in agreement with the green color of the film (Figure 2A). By using an equation previously reported,⁴⁸ it is possible to estimate the PANI film thickness (d_f) from the absorbance at 400 nm ($A_{400 \text{ nm}} = 5.4 \times 10^{-3} * d_f$ (in nm)). Finally, the thickness of the PANI film was estimated to be around $\sim 0.3 \mu\text{m}$.

The PET/PANI XPS spectrum presents a peak at a binding energy of ~ 400 eV (Figure 2B). This position is explained by the electrons emitted from the 1s orbitals of the nitrogen atoms in PANI. Furthermore, deconvolution of the N 1s peak revealed the presence of the characteristic PANI contributions: amino groups ($-\text{NH}-$) (~ 399.5 eV), imino groups ($=\text{N}-$) (~ 398.2 eV), and charged nitrogen moieties (~ 400.8 and 402.2 eV).⁴⁹

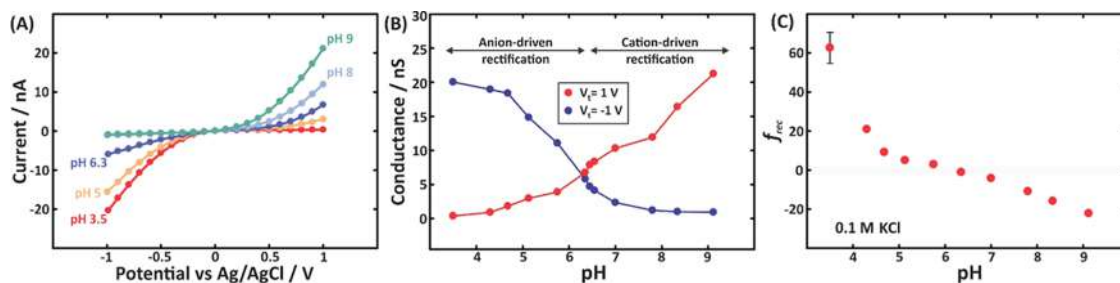


Figure 3. (A) I - V curves at different pH values of a nanochannel in a PET foil modified with PANI. (B) Dependence of the conductance on the pH of the medium. The red and blue curves correspond to the conductance at transmembrane voltages of 1 and -1 V, respectively. (C) Dependence of the rectification efficiency on the pH of the medium. The system shows a zwitterionic behavior. All measurements were carried out in a 0.1 M KCl solution.

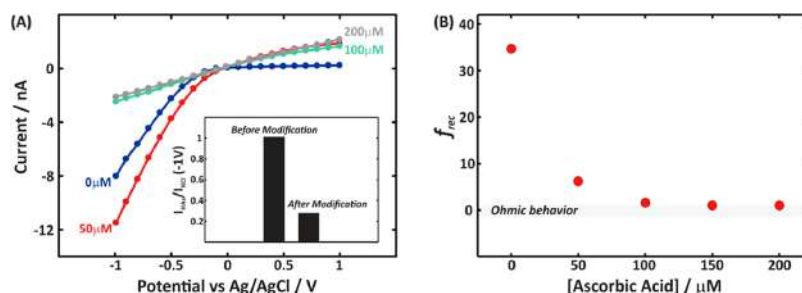


Figure 4. (A) I - V curves of a PANI-modified membrane recorded in the presence of different concentrations of ascorbic acid (0–200 μ M). The control experiment in the inset shows the currents of the nanochannel with and without PANI in the presence of 100 μ M AA, which reinforces the idea that this behavior is due to the reduction of the PANI film. (B) Variation in the rectification factor due to the presence of ascorbic acid. All curves were recorded in 0.1 M KCl at pH = 3.5.

The Raman spectrum of the bare foil shows the main PET bands: C=C stretching (1610 cm^{-1}), C=O stretching (1724 cm^{-1}), and stretching of C-C (ring) and C-O (1286 cm^{-1}) (Figure 2C). Thus, the bands of C=N stretching of the quinoid ring (1484 cm^{-1}), C-N stretching (1215 cm^{-1}), and C-H bending of the quinoid ring (1160 cm^{-1}) in the Raman spectrum of the modified foil give evidence of the successful synthesis of PANI. This spectrum presents the characteristic signals reported in previous works.^{50,51}

Water contact angle measurements provided values of 68 ± 3 and $55 \pm 6^\circ$ for PET and PET/PANI, respectively (Figure 2D). The modification with PANI obviously increases the wettability due to the higher hydrophilicity of PANI in comparison with that of PET. The average and standard deviation were obtained from five measures on different foil regions.

Iontronic Response of PANI-Functionalized PET Membranes. Acid–base equilibrium involves changes in the state of charge of PANI; therefore, the ionic transport of the PET/PANI membrane was studied as a function of pH. Figure 3A shows the I - V curves of a PET/PANI membrane recorded at different pH values. The I - V curves reveal that it is possible to vary the ion transport from anion-driven rectification to cation-driven rectification by changing the solution pH. Additionally, the iontronic output exhibits a nonrectifier behavior at pH = 6.3, which can be ascribed to the cancellation of the positive charge of PANI with the negative charge of nanochannel walls. Specifically, the high-positive-charge state of the PANI film at acidic pH causes a depletion (accumulation) of ions in the tip region for positive (negative) V_t , leading to a low (high) conductance with a predominant contribution of anions (Figure 3B). On the other hand, at basic pH values, PANI gets deprotonated and the effect of the negative charges on the

surface of the tip operates. In this case, the negative surface charge provided by the carboxylate groups is responsible for the depletion (accumulation) of ions at negative (positive) V_t values, and the current is mainly transported by cations. The appearance of a cation-driven behavior at high pH is consistent with the heterogeneous membrane configuration achieved by the chemical functionalization approach. Contrarily, a non-selective ohmic behavior is attained at high pH when metallized membranes are modified by electropolymerization as PET chemical groups are inaccessible after Au sputtering.⁴⁴ To quantify the rectification efficiency, the rectification factor (f_{rec}), defined as the ratio between the maximum currents in the high- and low-conductance branches ($|f_{\text{rec}}| > 1$) (eq 3), is analyzed. This parameter is of relevance because it provides a direct relation to the surface charge density, as evidenced in previous studies on ionic transport in SSN.^{17,52} Our asymmetric membranes exhibited a highly positive f_{rec} at acidic pH (Figure 3C). Taking into account that in the absence of redox agents emeraldine is expected to be the predominant state of PANI, the f_{rec} sign can be attributed to the high ratio of the protonated imine groups in the PANI film.⁵³ There is a wide range of $\text{p}K_a$ values reported for the emeraldine state ($\text{p}K_a \sim 4$ –8),⁵⁴ which is affected by the synthesis conditions.^{55,56} At pH = 3.5, a highly positive rectification is observed, whereas for pH > 3.5, the rectification decreases rapidly. This fact can be explained by both the deprotonation of PANI imine groups to uncharged moieties and the deprotonation of PET carboxyl groups to form negatively charged carboxylate groups. For pH = 6.3, the f_{rec} is around 1 owing to the partial compensation of the charges of the PANI and PET surfaces. This pH region is commonly called the “isoelectric region”.⁵² Finally, for pH > 6.3, the system shows a rectification of $f_{\text{rec}} < -1$, which became more negative as pH increases. This effect is due to the

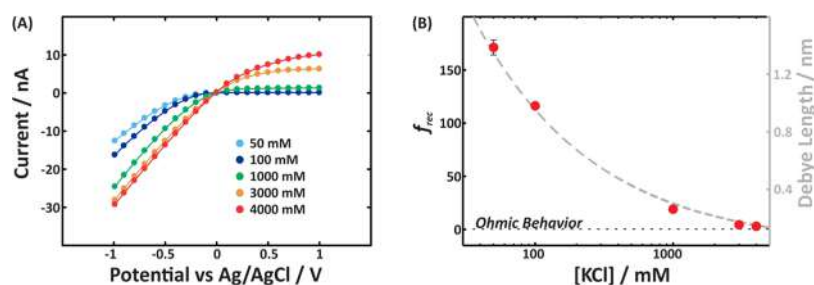


Figure 5. (A) I – V curves of a PANI-modified nanochannel membrane at different concentrations of KCl. (B) Rectification factor and Debye length at different concentrations of KCl. The PANI-functionalized single-pore membranes show good rectification efficiency even at high ionic strength. All curves were recorded in acidic media ($\text{pH} \sim 3$).

prevalence of PET carboxylate charges because of complete PANI deprotonation. In all cases, the system showed good reversibility and signal stability (Figure S2). The analysis of the anion-driven conductance (Figure 3B) allows us to determine an effective pK_a (≈ 6) for PANI in this system, which is consistent with the values reported for PANI films in other experimental configurations.⁵⁴

Redox Responsiveness. Taking into account that PANI ionic charge is influenced by the redox state, we also investigated the changes in the ionic transport in the presence of a reducing agent.^{44,57} I – V curves were recorded at different ascorbic acid (AA) concentrations in 0.1 M KCl at $\text{pH} = 3.5$ solution (Figure 4A). Concentrations greater than 100 μM AA yield an ohmic behavior with low currents. Figure 4B shows a great diminution of f_{rec} as the AA concentration increases. This change in iontronic behavior is not observed for the nonmodified PET membrane (inset in Figure 4A) and can be ascribed to the low ionic charge of the reduced leucoemeraldine ($\text{pK}_a < 1.5$).⁴⁴ On the other hand, the presence of AA under highly acidic conditions ($\text{pH} \sim 1.5$) reduces f_{rec} but does not lead to the complete loss of the rectifying behavior. This can be explained by the partial leucoemeraldine protonation at this lower pH , which is near the pK_a value of this redox form of PANI (Figure S3).⁵⁴

Rectification Behavior at High Salt Concentration. Usually, asymmetric nanochannels exhibit rectification if the tip diameter is comparable to the Debye length.¹⁸ Increasing the ionic strength (or salt concentration) leads to a decrease in the Debye length, which in turn reduces the rectification behavior. Thus, an increase of KCl concentration above 0.05 or 0.1 M usually produces a drop in rectification efficiencies.¹⁶ As a result, nanochannel-based nanofluidic devices do not efficiently rectify the ionic currents under symmetrical conditions of high ionic strength (e.g., in 1 M KCl). Based on the high rectification factors of the as-prepared PANI-functionalized PET membranes, we studied their rectification performance at different ionic strength values.

Figure 5A shows I – V curves of a PANI-modified nanochannel membrane at different KCl concentrations between 50 and 4000 mM. As expected, the increase in KCl concentration above 50 mM produces a diminution of f_{rec} (Figure 5B), but the rectifying values are surprisingly high with $f_{\text{rec}} \sim 20$ for 1 M KCl and the behavior is still non-ohmic at KCl concentrations as high as 3 and ~ 4 M. For qualitative comparison, the Debye length calculated for each KCl solution is added in Figure 5B. The Debye length is commonly used to characterize the electrical double layer (EDL) length. In the ionic transport across the nanochannels, a thicker EDL allows a more efficient co-ion exclusion and counterion enrichment, and therefore, a

surface charge governed the transport. In nanochannels with asymmetric geometries, the drop of the Debye length at high electrolyte concentration (>0.1 M) usually produces a loss of selectivity and, concomitantly, in the rectifying behavior. However, in this system, the rectifying behavior is preserved even at low Debye length values of ~ 0.17 nm. This means that the chemical modification with PANI promotes ionic current rectification even in pores with tip diameters greater than 400 times of the Debye length ($\lambda_D \sim 0.17$ nm in KCl ~ 3 M) (Figure S4). To the best of our knowledge, rectification at such high-ionic-strength solutions has not been reported previously in single-pore systems.

Furthermore, the rectification efficiency can be even improved by increasing the transmembrane voltage window (Figure 6). At 10 mM KCl, the PANI-functionalized membrane reached an $f_{\text{rec}} (\pm 5 \text{ V})$ of ~ 1350 , while for 50 mM KCl, the $f_{\text{rec}} (\pm 5 \text{ V})$ exceeded 900. These values by far exceed most of the previously reported rectification values.⁵⁸ For high KCl concentrations, f_{rec} was tripled by extending the transmembrane potential window to ± 2 V. These results support the application of PET/PANI heterogeneous membranes as a simple and suitable option for the robust design of high-ionic-strength nanofluidic diodes.

Surprisingly, the PANI-functionalized single-pore membrane keeps the zwitterionic behavior even at a high salt concentration of 1 M KCl (Figure 7). Thus, the system shows a pH -tunable ionic selectivity at high ionic strength (Figure 7A). At acidic pH , the system presents anionic selectivity due to charged PANI groups. Then, at $\text{pH} \sim 5$, the system exhibits nonselective (ohmic) behavior, which can be ascribed again to the compensation of the effects due to the positive and negative charges contributed by PANI and PET, respectively. Finally, at basic pH , the system shows cationic selectivity, probably due to the predominance of PET carboxylate groups. Concomitantly, the system allows turning the rectification from anion-driven rectification to cation-driven rectification by changing the solution pH even at high ionic strength (Figure 7B,C). This behavior, together with the great reproducibility and robustness (Table S1), makes the PET/PANI membranes even more interesting for the design of versatile platforms with accurate control of ion transport in a wide range of environmental conditions.

Blue Energy Harvesting Performance. Propelled by these interesting nanofluidic properties and taking into account the great interest in the development of new ways of low-cost environmentally friendly energy production, the performance of the PET/PANI membrane as an ion-selective membrane in reverse electrodialysis was evaluated. When a permselective membrane is placed as a separator between two salt solutions

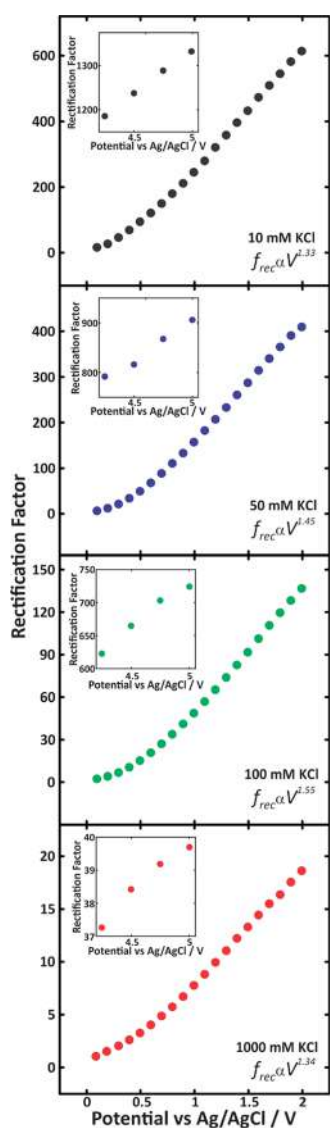


Figure 6. Rectification factor f_{rec} as a function of the transmembrane voltage for different KCl concentrations: 10 mM (black), 50 mM (blue), 100 mM (green), and 1000 mM (red) at pH \sim 3. The dependence of f_{rec} follows a voltage power law with an exponent between 1.33 and 1.55. The complete experimental data of the I - V curves are shown in Figure S5.

with different activities, an osmotic current (i_0) is generated, which is dominated by one ion species due to the ion-selective

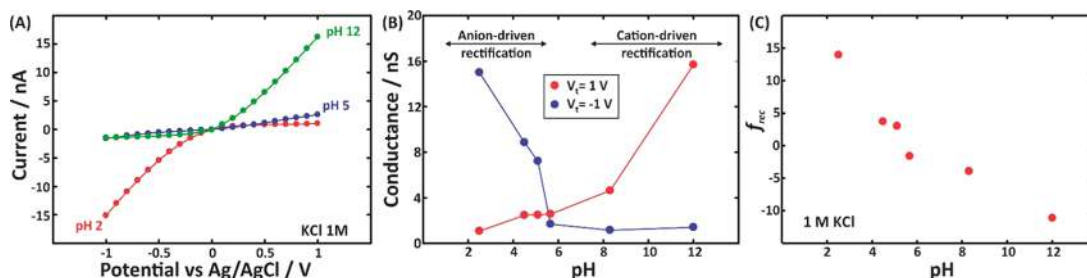


Figure 7. (A) I - V curves of a PANI-modified nanochannel membrane at 1 M KCl for different pH values. (B) Dependence of the conductance on the pH of the medium. The red and blue curves correspond to the conductance at transmembrane voltages of 1 and -1 V, respectively. (C) Variations of the rectification factor at different pH conditions. The system keeps the zwitterionic behavior even at high ionic strength. All measurements were carried out in 1 M KCl.

nature of the membrane.^{59,60} Additionally, the charge imbalance generates a diffusion voltage (E_{diff}). This fact makes it possible to generate electrical energy from nanofluidic devices using a salt concentration gradient. Having this application in mind, a bullet-shaped nanochannel foil modified with PANI was mounted in a two-chamber electrolytic cell. The two chambers were filled with KCl solutions of different concentrations (Figure 8). In all cases, the membrane was

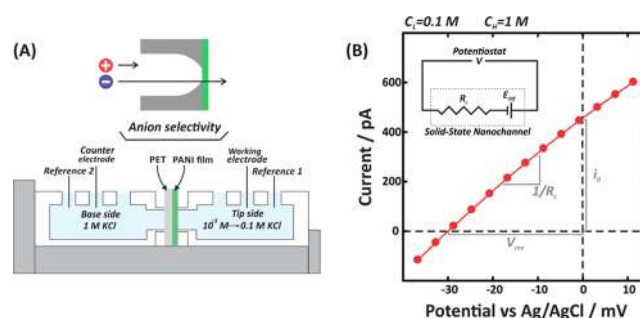


Figure 8. (A) Scheme of the conductivity cell where the left chamber contained a fixed high KCl concentration of $C_H = 1$ M and the chamber facing the membrane with the small, PANI-modified nanochannel was filled with different KCl concentrations C_L between 0.001 and 0.1 M. (B) I - V curve for a nanochannel exposed to a concentration gradient of $C_H = 1$ M and $C_L = 0.1$ M. Values for i_0 , R_c , and V_{rev} (E_{diff}) are indicated. The electric circuit equivalent to the experimental setup is shown too.

placed with the large pore opening toward the chamber with the KCl solution of high concentration (C_H) (fixed at 1 M KCl), whereas the membrane surface with the small channel tip with the PANI film was in contact with the KCl solution of low concentration of KCl (C_L) (variable from 10^{-3} to 0.1 M) (Figure 8A). As shown earlier, this configuration provides better performance.^{61,62} The conductometric measurements are characterized by the shift of the I - V curve with respect to $I = 0$ and $V = 0$ (Figure 8B). This effect is described as follows (see the reference for further details)^{35,61}

$$V = V_{rev} + IR_c \quad (1)$$

where the zero-volt current (I_{ZY}), the channel resistance (R_c), and the open-circuit voltage (V_{rev}) values were obtained from the I - V curves recorded under asymmetric concentration conditions (Figure 8B).

It should be noted that the potential drop of the two Ag/AgCl electrodes (E_{redox}) due to the contact with different KCl concentrations could contribute to V_{rev} .⁶³ Thus, commonly,

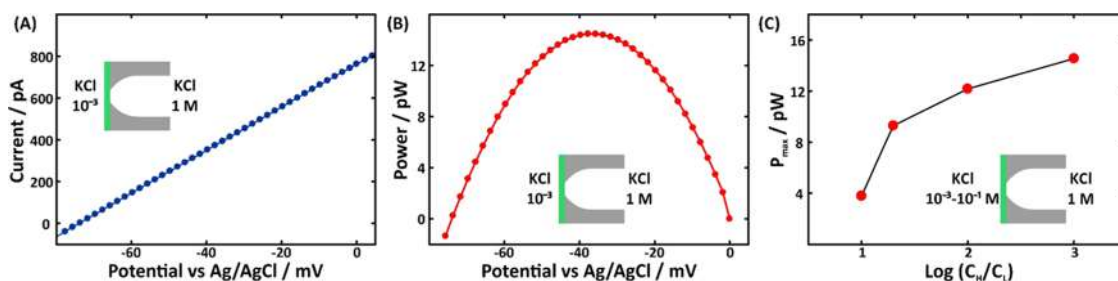


Figure 9. (A) I – V curve under a 1000-fold gradient concentration across a PET/PANI single nanochannel. (B) Power P versus voltage curve under a 1000-fold concentration gradient. The PANI-functionalized single-channel membrane exhibits excellent performance as an energy conversion system. (C) Maximum power P_{\max} as a function of the applied concentration gradient ($\log(C_H/C_L)$). All curves were recorded using KCl electrolyte at pH = 3.5.

the latter contribution is subtracted to obtain only the contribution of the ionic selectivity of the nanochannel (E_{diff}). However, in this work, both Ag/AgCl electrodes were immersed in 3 M KCl solutions (salt bridge), yielding negligible E_{redox} and liquid junction potential contribution.^{31,35} It is still necessary to subtract the contribution coming from differences in the reference electrodes. However, this value was lower than 5 mV and did not depend on the KCl concentration, so we considered $V_{\text{rev}} \approx E_{\text{diff}}$ and $I_{\text{ZV}} \approx i_0$ (Figure 8B).

The energy conversion performance was evaluated by the I – V curves recorded in KCl (pH \sim 3.5). At this pH condition, PANI is found in a high ionic charge state, and therefore, the nanofluidic transport is selective to anions (high $|E_{\text{diff}}|$). Under this condition, the gradient concentration will promote the generation of ionic flux from the base side (high concentration) to the tip side (low concentration), but the anion selectivity of the modified nanochannel will partially avoid cation transport. Figure 9 shows the energy conversion performance of the PANI-functionalized single-pore membrane. As previously mentioned, the I – V curve exhibits a closed-circuit current produced by the ionic flux from the base side to the tip side and, concomitantly, an open-circuit potential different from 0 (Figure 9A).

Usually, the performance of energy conversion systems is evaluated by means of the power (P). This parameter is defined as $P = V \cdot I$. Taking into account that the maximum power is obtained when $V = 0.5 E_{\text{diff}}$ the maximum power (P_{\max}) is defined as (see the references for further details)^{21,35,64}

$$P_{\max} = \frac{E_{\text{diff}}^2}{4R_c} \quad (2)$$

The power–voltage curve presented in Figure 9B shows a maximum of $P_{\max} = 15$ pW at about 37 mV under a 1000-fold gradient difference and pH = 3.5. Figure 9C presents the maximum power obtained by eq 2 for different concentration gradients. The performance of the nanofluidic energy conversion system can obviously be optimized by increasing the gradient concentration. A higher concentration difference between the half cells produces a higher ionic flux and also increases the E_{diff} (Figure S6).^{61,63} This maximum power exceeds those obtained for similar systems at acidic pH (Table S2). Furthermore, our values are in the order of those previously reported at neutral and basic pH using track-etched nanochannels (Table S2)^{21,31,33,34} and could be even improved by adjusting the opening diameters, the salt nature, and the shape of the pore, among other design parameters.^{31,35,65,66}

However, in contrast to previously reported systems based on the negatively charged PET, the present design allows operating in an acidic medium, which, considering the wide spectrum of solutions available for reverse electrodialysis operation, is an interesting way of exploiting industrial acidic waste.³⁷ This effect can be ascribed to the combination of bullet-shaped geometry and a highly charged PANI film (Table S2 and Figure S7). On one side, the bullet-shaped geometry promotes an increment in P_{\max} due to the maximization of the effective size and its concomitant maximization of i_0 . On the other side, the inclusion of the PANI film on the tip side via chemical synthesis promotes an increment of 100% in terms of P_{\max} in relation to that obtained for a nonmodified bullet-shaped nanochannel (Figure S7). Besides these interesting results, the challenge is to transfer our laboratory array to a macroscale system, which is not a trivial task.^{67,68} In the recent past, researchers have obtained attractive results by transferring energy conversion systems to multipore track-etched foils.³⁵ Therefore, taking into account that ion-track-etching allows generating a great number of nanochannels in a small area (for example, 10^9 channels per cm^2), this design is a suitable option for a new generation of renewable energy in microsystems.

Experimental Section. Chemicals. Aniline and APS were purchased from Sigma-Aldrich, and KCl, NaOH, H_2SO_4 , and HCl were from Anedra. All chemicals were of analytical grade. All experiments were carried out using Milli-Q water (\sim 18 M Ω cm).

Etching. Bullet-shaped nanochannels were obtained by the ion-track-etching method, as reported in detail elsewhere.^{35,69} Poly(ethylene terephthalate) (PET) foils were irradiated with a single-high-energy Au ion (energy of \sim 2.2 GeV) at the linear accelerator UNILAC of the GSI Helmholtz Center for Heavy Ion Research, Darmstadt, Germany. Then, an asymmetric surfactant-assisted chemical etching was performed to convert the ion track into a bullet-shaped nanochannel.³⁵ For this, one side of the foil was exposed to 6 M NaOH (base side), whereas the other side was exposed to a mixture of 6 M NaOH and surfactant Dowfax 2a1 0.05% (tip side). The addition of a surfactant leads to a bullet-like geometry of the small tip of the nanochannel. The etching time and temperature were 6 min and 60 $^\circ\text{C}$, respectively. Under these conditions, channels with a tip diameter of \sim 70 nm and a base diameter of \sim 300 nm are obtained (Figure S1).

Modification. Bullet-shaped nanochannels were functionalized onto the tip side of the PET foil with polyaniline (PANI). The chemical synthesis was performed by exposing the foil to an aqueous solution of aniline (5 mM) and APS (5 mM) in 0.5 M H_2SO_4 for 3 h at room temperature.

Membrane Characterization. Raman spectra were recorded using a BW46S-785S model Raman spectrometer (i-Raman, BWTEK) with an excitation laser of 785 nm. Contact angles were measured using a Ramé-Hart contact angle system (Model 290) by dispensing 1 μ L droplets of Milli-Q. UV–vis absorption spectra were acquired with a Perkin-Elmer Lambda 35 UV–vis spectrometer. X-ray photoelectron spectroscopy (XPS) was performed using a SPECS SAGE HR 100 system spectrometer with a Mg K α (1253.6 eV) X-ray source at 12.5 kV and 10 mA.

Current–Voltage (I – V) Measurements. Conductometric measurements were performed using a four-electrode arrangement connected to a Gamry Reference 600 potentiostat: working Pt, reference 1: Ag/AgCl immersed in a solution of 3 M KCl; counter-electrode Pt, reference 2: Ag/AgCl immersed in a solution of 3 M KCl. The four-electrode array allowed us to correlate I – V curve variations to changes of the nanochannel.⁶⁹

Routine measurements were performed in KCl with a scan rate of 100 mV/s and a transmembrane voltage limit of ± 1 V, unless otherwise indicated. The working electrode was placed on the tip side of the membrane. KCl solutions were adjusted to the desired pH by adding diluted solutions of HCl and KOH.

The energy conversion performances were evaluated by applying concentration gradients of KCl solutions. The low concentration was placed on the tip side, whereas the high concentration was fixed at 1 M on the base side. These solutions were fixed at pH ~ 3.5 by adding the HCl solution. Transmembrane voltage routines were performed with a scan rate of 10 mV/s and potential limits of 0.15 and -0.15 V.

Rectification Factor (f_{rec}). The rectification efficiency was characterized by means of the rectification factor. This was calculated as the ratio of the absolute currents in high- and low-conductance states (eq 3).⁷⁰ If the high-conductance state was found at positive potentials, the f_{rec} was multiplied by -1 . This allowed us to relate the f_{rec} sign with the charge polarity of the nanochannel walls

$$f_{\text{rec}} = \pm \frac{|i(\text{high conductance})|}{|i(\text{low conductance})|} \quad (3)$$

Conclusions. In summary, we have developed a chemical approach for producing a membrane system with enhanced current rectification properties by means of a one-step PANI functionalization of the tip of a single bullet-shaped nanochannel in PET foils. This simple modification approach allows the control of ion transport by both pH and redox effectors. The whole system exhibits zwitterionic behavior even at high ionic concentrations (1 M KCl) as a consequence of the simultaneous influence of the charges on the etched nanopore wall and the PANI film deposited on the tip face of the membrane. This particular configuration allows achieving an anion-driven rectification at pH < 5 , a nonrectifying behavior at about pH 6, and a cation-driven rectification at pH > 7 . Furthermore, the presence of ascorbic acid leads to the chemical reduction of PANI, causing a decrease of the surface net charge and decreasing ionic rectification. The system displays very high rectification factors and tunable ionic transport even in solutions with high salt concentrations. In addition, the PET/PANI asymmetric membrane worked as an efficient salinity gradient-based energy conversion device even in acidic concentrated salt solutions, opening the door to

applications under severe acidic operating conditions. The current challenge involves the transference of this single-nanochannel design to the macroscale using foils with high channel densities (e.g. 10^9 – 10^{10} channels/cm²). We believe that the improved ionic transport features achieved by the PANI functionalization method will propel its implementation in other nanofluidics applications such as filtration, energy conversion, and nanoelectronics.

■ ASSOCIATED CONTENT

Supporting Information

The Supporting Information is available free of charge at <https://pubs.acs.org/doi/10.1021/acsami.0c05102>.

SEM images, cyclability toward pH changes, redox performance at acidic pH, I – V curves at different salt concentrations, energy conversion performance of the unmodified PET channel, and comparison of energy conversion performance among different systems (PDF)

■ AUTHOR INFORMATION

Corresponding Authors

Waldemar Marmisollé – Instituto de Investigaciones Físicoquímicas Teóricas y Aplicadas (INIFTA), Departamento de Química, Facultad de Ciencias Exactas, Universidad Nacional de La Plata (UNLP), CONICET, 1900 La Plata, Argentina; orcid.org/0000-0003-0031-5371; Email: wmarmi@inifta.unlp.edu.ar

Omar Azzaroni – Instituto de Investigaciones Físicoquímicas Teóricas y Aplicadas (INIFTA), Departamento de Química, Facultad de Ciencias Exactas, Universidad Nacional de La Plata (UNLP), CONICET, 1900 La Plata, Argentina; orcid.org/0000-0002-5098-0612; Email: azzaroni@inifta.unlp.edu.ar; <https://softmatter.quimica.unlp.edu.ar/>

Authors

Gregorio Laucirica – Instituto de Investigaciones Físicoquímicas Teóricas y Aplicadas (INIFTA), Departamento de Química, Facultad de Ciencias Exactas, Universidad Nacional de La Plata (UNLP), CONICET, 1900 La Plata, Argentina

María Eugenia Toimil-Molares – GSI Helmholtzzentrum für Schwerionenforschung, 64291 Darmstadt, Germany

Christina Trautmann – GSI Helmholtzzentrum für Schwerionenforschung, 64291 Darmstadt, Germany; Technische Universität Darmstadt, Materialwissenschaft, 64287 Darmstadt, Germany

Complete contact information is available at: <https://pubs.acs.org/doi/10.1021/acsami.0c05102>

Notes

The authors declare no competing financial interest.

■ ACKNOWLEDGMENTS

G.L. acknowledges a doctoral scholarship from CONICET. W.M. and O.A. are CONICET fellows and acknowledge financial support from the Universidad Nacional de La Plata (PID-X867) and ANPCyT (PICT-2017-1523 and PICT-2016-1680). C.T. and M.E.T.-M. acknowledge support by the LOEWE project iNAPO funded by the Hessen State Ministry of Higher Education, Research and Arts. The irradiated PET foils are part of the experiment UMAT, which was performed at the beam line X0 at the GSI Helmholtzzentrum für

Schwerionenforschung, Darmstadt (Germany), in the frame of FAIR Phase-0.

REFERENCES

- (1) Dekker, C. Solid-State Nanopores. *Nat. Nanotechnol.* **2007**, *2*, 209–215.
- (2) Zhang, Z.; Wen, L.; Jiang, L. Bioinspired Smart Asymmetric Nanochannel Membranes. *Chem. Soc. Rev.* **2018**, *47*, 322–356.
- (3) Pérez-Mitta, G.; Peinetti, A. S.; Cortez, M. L.; Toimil-Molares, M. E.; Trautmann, C.; Azzaroni, O. Highly Sensitive Biosensing with Solid-State Nanopores Displaying Enzymatically Reconfigurable Rectification Properties. *Nano Lett.* **2018**, *18*, 3303–3310.
- (4) Howorka, S.; Siwy, Z. Nanopore Analytics: Sensing of Single Molecules. *Chem. Soc. Rev.* **2009**, *38*, 2360–2384.
- (5) Xie, G.; Wen, L.; Jiang, L. Biomimetic Smart Nanochannels for Power Harvesting. *Nano Res.* **2016**, *9*, 59–71.
- (6) Xie, G.; Li, P.; Zhang, Z.; Xiao, K.; Kong, X. Y.; Wen, L.; Jiang, L. Skin-Inspired Low-Grade Heat Energy Harvesting Using Directed Ionic Flow through Conical Nanochannels. *Adv. Energy Mater.* **2018**, *8*, No. 1800459.
- (7) Heiranian, M.; Farimani, A. B.; Aluru, N. R. Water Desalination with a Single-Layer MoS₂ Nanopore. *Nat. Commun.* **2015**, *6*, No. 8616.
- (8) Hou, X.; Guo, W.; Jiang, L. Biomimetic Smart Nanopores and Nanochannels. *Chem. Soc. Rev.* **2011**, *40*, 2385–2401.
- (9) Pérez-Mitta, G.; Albesa, A. G.; Trautmann, C.; Toimil-Molares, M. E.; Azzaroni, O. Bioinspired Integrated Nanosystems Based on Solid-State Nanopores: “Iontronic” Transduction of Biological, Chemical and Physical Stimuli. *Chem. Sci.* **2017**, *8*, 890–913.
- (10) Pérez-Mitta, G.; Toimil-Molares, M. E.; Trautmann, C.; Marmisollé, W. A.; Azzaroni, O. Molecular Design of Solid-State Nanopores: Fundamental Concepts and Applications. *Adv. Mater.* **2019**, *31*, No. 1901483.
- (11) Laucirica, G.; Cayón, V. M.; Toum Terrones, Y.; Cortez, M. L.; Toimil-Molares, M. E.; Trautmann, C.; Marmisollé, W. A.; Azzaroni, O. Electrochemically Addressable Nanofluidic Devices Based on PET Nanochannels Modified with Electropolymerized Poly-o-Aminophenol Films. *Nanoscale* **2020**, *12*, 6002–6011.
- (12) Hou, X. Smart Gating Multi-Scale Pore/Channel-Based Membranes. *Adv. Mater.* **2016**, *28*, 7049–7064.
- (13) Xiao, K.; Wen, L.; Jiang, L. Biomimetic Solid-State Nanochannels: From Fundamental Research to Practical Applications. *Small* **2016**, *12*, 2810–2831.
- (14) Tagliazucchi, M.; Szeleifer, I. Transport Mechanisms in Nanopores and Nanochannels: Can We Mimic Nature? *Mater. Today* **2015**, *18*, 131–142.
- (15) Vlassiok, I.; Siwy, Z. S. Nanofluidic Diode. *Nano Lett.* **2007**, *7*, 552–556.
- (16) Siwy, Z. S. Ion-Current Rectification in Nanopores and Nanotubes with Broken Symmetry. *Adv. Funct. Mater.* **2006**, *16*, 735–746.
- (17) Xiong, T.; Zhang, K.; Jiang, Y.; Yu, P. Ion Current Rectification: From Nanoscale to Microscale. *Sci. China: Chem.* **2019**, 1–14.
- (18) Daiguji, H.; Yang, P.; Majumdar, A. Ion Transport in Nanofluidic Channels. *Nano Lett.* **2004**, *4*, 137–142.
- (19) Schoch, R. B.; Renaud, P. Ion Transport through Nanoslits Dominated by the Effective Surface Charge. *Appl. Phys. Lett.* **2005**, *86*, No. 253111.
- (20) Lin, C.; Yeh, L.; Siwy, Z. S. Voltage-Induced Modulation of Ionic Concentrations and Ion Current Rectification in Mesopores with Highly Charged Pore Walls. *J. Phys. Chem. Lett.* **2018**, *9*, 393–398.
- (21) Lin, C.; Combs, C.; Su, Y.; Yeh, L.; Siwy, Z. S. Rectification of Concentration Polarization in Mesopores Leads To High Conductance Ionic Diodes and High Performance Osmotic Power. *J. Am. Chem. Soc.* **2019**, *141*, 3691–3698.
- (22) Ge, Y.; Zhu, J.; Kang, M.; Xian, J.; An, Q.; Zhong, G. Ion Current Rectification in a Confined Conical Nanopore with High Solution Concentrations. *Mol. Simul.* **2016**, *42*, 942–947.
- (23) Gao, J.; Guo, W.; Feng, D.; Wang, H.; Zhao, D.; Jiang, L. High-Performance Ionic Diode Membrane for Salinity Gradient Power Generation. *J. Am. Chem. Soc.* **2014**, *136*, 12265–12272.
- (24) Schiedt, B.; Healy, K.; Morrison, A. P.; Neumann, R.; Siwy, Z. Transport of Ions and Biomolecules through Single Asymmetric Nanopores in Polymer Films. *Nucl. Instrum. Methods Phys. Res., Sect. B* **2005**, *236*, 109–116.
- (25) He, Y.; Gillespie, D.; Boda, D.; Vlassiok, I.; Eisenberg, R.; Siwy, Z. Tuning Transport Properties of Nanofluidic Devices with Local Charge Inversion. *J. Am. Chem. Soc.* **2009**, *131*, 5194–5202.
- (26) Zhu, X.; Hao, J.; Bao, B.; Zhou, Y.; Zhang, H.; Pang, J.; Jiang, Z.; Jiang, L. Unique Ion Rectification in Hypersaline Environment: A High-Performance and Sustainable Power Generator System. *Sci. Adv.* **2018**, *4*, No. eaau1665.
- (27) Karnik, R.; Duan, C.; Castelino, K.; Daiguji, H.; Majumdar, A. Rectification of Ionic Current in a Nanofluidic Diode. *Nano Lett.* **2007**, *7*, 547–551.
- (28) Hou, X.; Zhang, H.; Jiang, L. Building Bio-Inspired Artificial Functional Nanochannels: From Symmetric to Asymmetric Modification. *Angew. Chem., Int. Ed.* **2012**, *51*, 5296–5307.
- (29) Zhang, Q.; Kang, J.; Xie, Z.; Diao, X.; Liu, Z.; Zhai, J. Highly Efficient Gating of Electrically Actuated Nanochannels for Pulsatile Drug Delivery Stemming from a Reversible Wettability Switch. *Adv. Mater.* **2017**, *30*, No. 1703323.
- (30) Yameen, B.; Ali, M.; Neumann, R.; Ensinger, W.; Knoll, W.; Azzaroni, O. Synthetic Proton-Gated Ion Channels via Single Solid-State Nanochannels Modified with Responsive Polymer Brushes. *Nano Lett.* **2009**, *9*, 2788–2793.
- (31) Guo, W.; Cao, L.; Xia, J.; Nie, F. Q.; Wen, M.; Xue, J.; Song, Y.; Zhu, D.; Wang, Y.; Jiang, L. Energy Harvesting with Single-Ion-Selective Nanopores: A Concentration-Gradient-Driven Nanofluidic Power Source. *Adv. Funct. Mater.* **2010**, *20*, 1339–1344.
- (32) Zhang, Z.; Kong, X. Y.; Xiao, K.; Liu, Q.; Xie, G.; Li, P.; Ma, J.; Tian, Y.; Wen, L.; Jiang, L. Engineered Asymmetric Heterogeneous Membrane: A Concentration-Gradient-Driven Energy Harvesting Device. *J. Am. Chem. Soc.* **2015**, *137*, 14765–14772.
- (33) Ma, T.; Balanzat, E.; Janot, J.-M.; Balme, S. Nanopore Functionalized by Highly Charged Hydrogels for Osmotic Energy Harvesting. *ACS Appl. Mater. Interfaces* **2019**, *11*, 12578–12585.
- (34) Balme, S.; Ma, T.; Balanzat, E.; Janot, J. Large Osmotic Energy Harvesting from Functionalized Conical Nanopore Suitable for Membrane Applications. *J. Membr. Sci.* **2017**, *544*, 18–24.
- (35) Laucirica, G.; Albesa, A. G.; Toimil-Molares, M. E.; Trautmann, C.; Marmisollé, W. A.; Azzaroni, O. Shape Matters: Enhanced Osmotic Energy Harvesting in Bullet-Shaped Nanochannels. *Nano Energy* **2020**, *71*, No. 104612.
- (36) Siria, A.; Poncharal, P.; Bianco, A.; Fulcrand, R.; Blasé, X.; Purcell, S. T.; Bocquet, L. Giant Osmotic Energy Conversion Measured in a Single Transmembrane Boron Nitride Nanotube. *Nature* **2013**, *494*, 455–458.
- (37) Xin, W.; Zhang, Z.; Huang, X.; Hu, Y.; Zhou, T.; Zhu, C.; Kong, X.; Jiang, L.; Wen, L. High-Performance Silk-Based Hybrid Membranes Employed for Osmotic Energy Conversion. *Nat. Commun.* **2019**, *10*, No. 3876.
- (38) Yang, H.-C.; Xie, Y.; Hou, J.; Cheetham, A. K.; Chen, V.; Darling, S. B. Janus Membranes: Creating Asymmetry for Energy Efficiency. *Adv. Mater.* **2018**, *30*, No. 1801495.
- (39) Zhang, Z.; Sui, X.; Li, P.; Xie, G.; Kong, X. Y.; Xiao, K.; Gao, L.; Wen, L.; Jiang, L. Ultrathin and Ion-Selective Janus Membranes for High-Performance Osmotic Energy Conversion. *J. Am. Chem. Soc.* **2017**, *139*, 8905–8914.
- (40) Manohar, S. K.; Macdiarmid, A. G.; Epstein, A. J. Polyaniline: Pernigraniline, an Isolable Intermediate in the Conventional Chemical Synthesis of Emeraldine. *Synth. Met.* **1991**, *41*, 711–714.
- (41) Inzelt, G. *Conducting Polymers: A New Era in Electrochemistry*; Springer-Verlag: Berlin, Heidelberg, 2008.

- (42) Marmisollé, W. A.; Inés Florit, M.; Posadas, D. The Coupling among Electron Transfer, Deformation, Screening and Binding in Electrochemically Active Macromolecules. *Phys. Chem. Chem. Phys.* **2010**, *12*, 7536–7544.
- (43) Marmisollé, W. A.; Florit, M. I.; Posadas, D. Coupling between Proton Binding and Redox Potential in Electrochemically Active Macromolecules. The Example of Polyaniline. *J. Electroanal. Chem.* **2013**, *707*, 43–51.
- (44) Pérez-Mitta, G.; Marmisollé, W. A.; Trautmann, C.; Toimil-Molares, M. E.; Azzaroni, O. Nanofluidic Diodes with Dynamic Rectification Properties Stemming from Reversible Electrochemical Conversions in Conducting Polymers. *J. Am. Chem. Soc.* **2015**, *137*, 15382–15385.
- (45) Apel, P. Y.; Blonskaya, I. V.; Dmitriev, S. N.; Orelvitch, O. L.; Presz, A.; Sartowska, B. A. Fabrication of Nanopores in Polymer Foils with Surfactant-Controlled Longitudinal Profiles. *Nanotechnology* **2007**, *18*, No. 305302.
- (46) Feast, W. J.; Tsibouklis, J.; Pouwer, K. L.; Groenendaal, L.; Meijer, E. W. Synthesis, Processing and Material Properties of Conjugated Polymers. *Polymer* **1996**, *37*, 5017–5047.
- (47) Belkova, A. A.; Sergeeva, A. I.; Apel, P. Y.; Beklemishev, M. K. Diffusion of Aniline through a Polyethylene Terephthalate Track-Etched Membrane. *J. Membr. Sci.* **2009**, *330*, 145–155.
- (48) Sapurina, L.; Riede, A.; Stejskal, J. In-Situ Polymerized Polyaniline Films - 3. Film Formation. *Synth. Met.* **2001**, *123*, 503–507.
- (49) Golczak, S.; Kancierzewska, A.; Fahlman, M.; Langer, K.; Langer, J. J. Comparative XPS Surface Study of Polyaniline Thin Films. *Solid State Ionics* **2008**, *179*, 2234–2239.
- (50) Čirić-Marjanović, G.; Trchová, M.; Stejskal, J. The Chemical Oxidative Polymerization of Aniline in Water: Raman Spectroscopy. *J. Raman Spectrosc.* **2008**, *39*, 1375–1387.
- (51) Lindfors, T.; Ivaska, A. Raman Based PH Measurements with Polyaniline. *J. Electroanal. Chem.* **2005**, *580*, 320–329.
- (52) Pérez-Mitta, G.; Albesa, A.; Gilles, F. M.; Toimil-Molares, M. E.; Trautmann, C.; Azzaroni, O. Noncovalent Approach toward the Construction of Nanofluidic Diodes with PH-Reversible Rectifying Properties: Insights from Theory and Experiment. *J. Phys. Chem. C* **2017**, *121*, 9070–9076.
- (53) MacDiarmid, A. G. “Synthetic Metals”: A Novel Role for Organic Polymers (Nobel Lecture). *Angew. Chem., Int. Ed.* **2001**, *40*, 2581–2590.
- (54) Marmisollé, W. A.; Florit, M. I.; Posadas, D. Acid-Base Equilibrium in Conducting Polymers. The Case of Reduced Polyaniline. *J. Electroanal. Chem.* **2014**, *734*, 10–17.
- (55) Okamoto, H.; Kotaka, T. Effect of Counter Ions in Electrochemical Polymerization Media on the Structure and Responses of the Product Polyaniline Films: III. Structure and Properties of Polyaniline Films Prepared via Electrochemical Polymerization. *Polymer* **1999**, *40*, 407–417.
- (56) Lindfors, T.; Harju, L. Determination of the Protonation Constants of Electrochemically Polymerized Poly(Aniline) and Poly(o-Methylaniline) Films. *Synth. Met.* **2008**, *158*, 233–241.
- (57) Bossi, A.; Piletsky, S. A.; Piletska, E. V.; Righetti, P. G.; Turner, A. P. F. An Assay for Ascorbic Acid Based on Polyaniline-Coated Microplates. *Anal. Chem.* **2000**, *72*, 4296–4300.
- (58) Yao, H.; Zeng, J.; Zhai, P.; Li, Z.; Cheng, Y.; Liu, J.; Mo, D.; Duan, J.; Wang, L.; Sun, Y.; Liu, J. Large Rectification Effect of Single Graphene Nanopore Supported by PET Membrane. *ACS Appl. Mater. Interfaces* **2017**, *9*, 11000–11008.
- (59) Siwy, Z.; Kosińska, I. D.; Fuliński, A.; Martin, C. R. Asymmetric Diffusion through Synthetic Nanopores. *Phys. Rev. Lett.* **2005**, *94*, 1–4.
- (60) Cervera, J.; Ramirez, P.; Mafe, S.; Stroeve, P. Asymmetric Nanopore Rectification for Ion Pumping, Electrical Power Generation, and Information Processing Applications. *Electrochim. Acta* **2011**, *56*, 4504–4511.
- (61) Cervera, J.; Alcaraz, A.; Schiedt, B.; Neumann, R.; Ramírez, P. Asymmetric Selectivity of Synthetic Conical Nanopores Probed by Reversal Potential Measurements. *J. Phys. Chem. C* **2007**, *111*, 12265–12273.
- (62) Hsu, J. P.; Lin, S. C.; Lin, C. Y.; Tseng, S. Power Generation by a PH-Regulated Conical Nanopore through Reverse Electrodialysis. *J. Power Sources* **2017**, *366*, 169–177.
- (63) Bard, A. J.; Faulkner, L. R. *Electrochemical Methods. Fundamentals and Applications*, 2nd ed.; Harris, D., Swain, E., Eds.; Wiley: New York, 2001.
- (64) Ouyang, W.; Wang, W.; Zhang, H.; Wu, W.; Li, Z. Nanofluidic Crystal: A Facile, High-Efficiency and High-Power-Density Scaling up Scheme for Energy Harvesting Based on Nanofluidic Reverse Electrodialysis. *Nanotechnology* **2013**, *24*, No. 345401.
- (65) Cao, L.; Guo, W.; Ma, W.; Wang, L.; Xia, F.; Wang, S.; Wang, Y.; Jiang, L.; Zhu, D. Towards Understanding the Nanofluidic Reverse Electrodialysis System: Well Matched Charge Selectivity and Ionic Composition. *Energy Environ. Sci.* **2011**, *4*, 2259–2266.
- (66) Hsu, J.-P. P.; Su, T.-C. C.; Lin, C.-Y. Y.; Tseng, S. Power Generation from a PH-Regulated Nanochannel through Reverse Electrodialysis: Effects of Nanochannel Shape and Non-Uniform H⁺ Distribution. *Electrochim. Acta* **2019**, *294*, 84–92.
- (67) Su, J.; Ji, D.; Tang, J.; Li, H.; Feng, Y.; Cao, L.; Jiang, L.; Guo, W. Anomalous Pore-Density Dependence in Nanofluidic Osmotic Power Generation. *Chin. J. Chem.* **2018**, *36*, 417–420.
- (68) Kwon, K.; Lee, S. J.; Li, L.; Han, C.; Kim, D. Energy Harvesting System Using Reverse Electrodialysis with Nanoporous Polycarbonate Track-Etch Membranes. *Int. J. Energy Res.* **2014**, *38*, 530–537.
- (69) Laucirica, G.; Pérez-Mitta, G.; Toimil-Molares, M. E.; Trautmann, C.; Marmisollé, W. A.; Azzaroni, O. Amine-Phosphate Specific Interactions within Nanochannels: Binding Behavior and Nanoconfinement Effects. *J. Phys. Chem. C* **2019**, *123*, 28997–29007.
- (70) Laucirica, G.; Marmisollé, W. A.; Toimil-Molares, M. E. E.; Trautmann, C.; Azzaroni, O. Redox-Driven Reversible Gating of Solid-State Nanochannels. *ACS Appl. Mater. Interfaces* **2019**, *11*, 30001–30009.